Title	Comparison of radar-based microwave imaging algorithms applied to experimental breast phantoms
Author(s)	Elahi, Muhammad Adnan; Lavoie, B. R.; Porter, Emily; Glavin, Martin; Jones, E.; Fear, E. C.; O'Halloran, Martin
Publication Date	2017-08-19
Publication Information	Elahi, M. A., Lavoie, B. R., Porter, E., Glavin, M., Fear, E.C., & O'Halloran, M. (2017). Comparison of radar-based microwave imaging algorithms applied to experimental breast phantoms. Paper presented at the 32nd Internal Union of Radio Science General Assembly & Scientific Symposium (URSI 2017 GASS), Montreal, 19-26 August.
Publisher	Union Radio-Scientifique Internationale
Link to publisher's version	http://www.ursi.org/proceedings/procGA17/papers/Paper_K7-3(1103).pdf
Item record	http://hdl.handle.net/10379/7034

Comparison of Radar-based Microwave Imaging Algorithms applied to Experimental Breast Phantoms

M. A. Elahi[1], B. R. Lavoie[2], E. Porter[1], M. Glavin[1], E. Jones[1], E. C. Fear[2], and M. O'Halloran[1]

(1) Electrical and Electronic Engineering, National University of Ireland Galway, Galway, Ireland

(2) Dept. of Electrical and Computer Engineering, University of Calgary, AB, Canada

Abstract

Microwave imaging is a promising imaging modality for the early detection of breast cancer. The two most important signal processing components of a radar-based microwave imaging system are the early-time artifact removal and the image reconstruction algorithm. Several image reconstruction algorithms have been developed and their performance has been evaluated in a number of studies. However, most of these evaluation studies were either performed on numerical breast phantoms or used an idealized artifact removal algorithm. In this paper, a range of both data independent and data adaptive imaging algorithms are evaluated using experimental breast phantoms in combination with a realistic artifact removal algorithm. The clutter rejection capabilities of each algorithm are assessed in the presence of experimental noise and residual artifacts using a range of appropriate image quality metrics.

1 Introduction

The quality of a radar-based microwave breast image is largely dependent on the clutter rejection capability of the imaging algorithm and the efficacy of early-time artifact removal algorithm. A number of image reconstruction algorithms have been developed since the inception of radar-based microwave breast imaging using Confocal Microwave Imaging (CMI) [1]. The performance of a selection of these imaging algorithms has been evaluated in a number of studies [2–7]. However, most of the comparative studies evaluated a limited number of imaging algorithms [2]; used relatively simplistic numerical breast models [3–5]; and employed an idealized artifact removal algorithm [6–8].

The focus of this paper is to: (i) evaluate a broader number of image reconstruction algorithms for the microwave breast imaging that include both Data-Independent (DI) and Data Adaptive (DA) beamformers; (ii) use experimental breast phantoms to evaluate their performance in the presence of experimental noise; (iii) and use a realistic artifact removal algorithm to account for the impact of any residual artifacts on the image quality. The experimental breast phantoms used in this evaluation study were developed at the University of Calgary (UOFC) and scanned with the second generation Tissue Sensing Adaptive Radar (TSAR) prototype [9]. The early-time artifact is reduced using the Hybrid Artifact Removal (HAR) algorithm [10, 11]. The quality of the images reconstructed using the various imaging algorithms is evaluated using a number of appropriate image quality metrics.

2 Imaging Algorithms

The imaging algorithms examined in this paper are as follows: Delay-And-Sum (DAS) [1]; Delay-Multiply-And-Sum (DMAS) [6]; Improved Delay-And-Sum (IDAS) [6]; Coherence Factor based DAS (CF-DAS) [12]; Channel Ranked DAS (CR-DAS) [13]; and Robust Capon Beamformer (RCB) [3].

In the conventional DAS beamformer, the signals received at individual channels are time-aligned for a synthetic focal point $\vec{r}$. Next, the time-aligned signals are summed together. The reflections from the tumour are expected to add coherently. Conversely, the reflections from healthy tissues and any artifacts are expected to add incoherently. The energy of the summed signal (often computed over a time-window) is assigned to the intensity of the focal point under consideration, and the process is repeated for all focal points within the breast. More advanced algorithms are variants of the conventional DAS algorithm. The DMAS adds a pairing multiplication step to DAS that synthetically increases the sample size resulting in better clutter suppression. The IDAS and the CF-DAS add coherence quality-based weighting factors in the DAS to improve the imaging quality. The CR-DAS scales each individual signal with a weighting factor to reward channels with shorter propagation path, assuming that the signals at such channels would have suffered less attenuation and would contain stronger tumour responses [13]. Finally, the RCB estimates the signal energy for each each synthetic focal point by adaptively selecting a weight vector for the received signals. The weight vector is chosen to attenuate the interference and noise while preserving the signal of interest.

3 Experimental Phantoms

The experimental breast phantoms used in this paper have been described in [9]. The breast phantoms include ma-
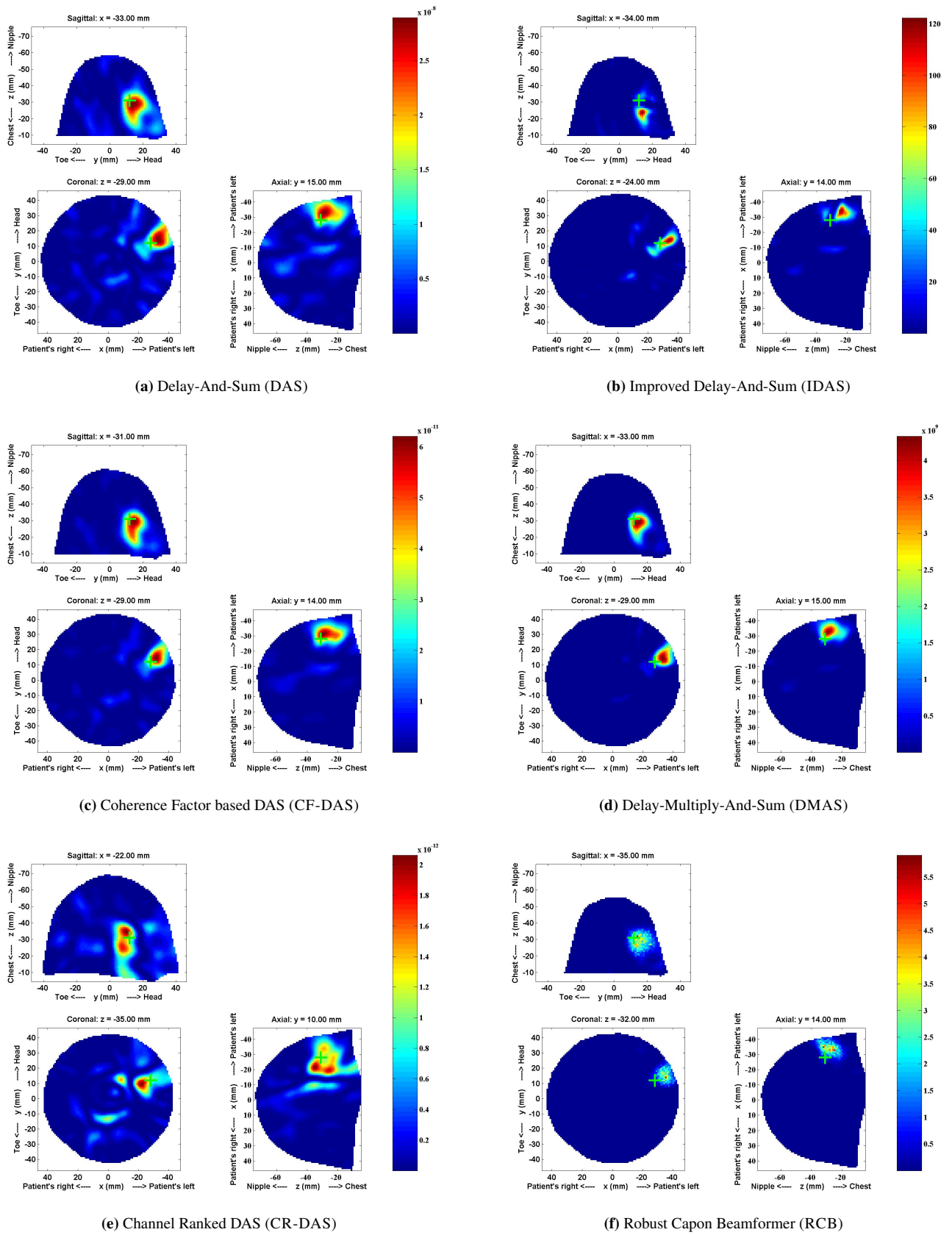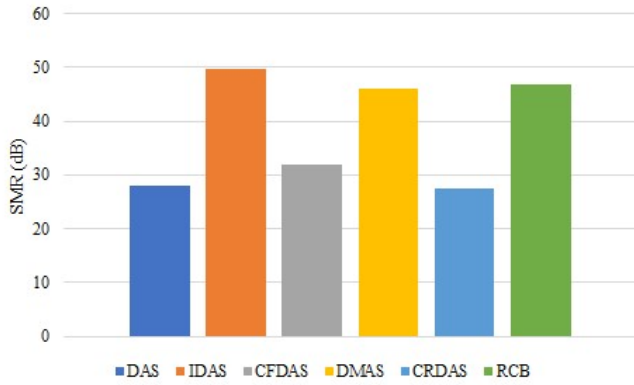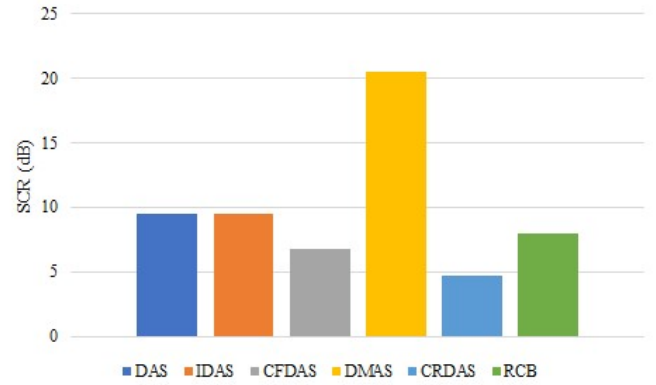
(a) Delay-And-Sum (DAS)

(b) Improved Delay-And-Sum (IDAS)

(c) Coherence Factor based DAS (CF-DAS)

(d) Delay-Multiply-And-Sum (DMAS)

(e) Channel Ranked DAS (CR-DAS)

(f) Robust Capon Beamformer (RCB)

Figure 1. Microwave images of *E2*.

(a) SMR averaged across both phantoms.

(b) SCR averaged across both phantoms.

terials representing skin tissue, fatty tissue, glandular tissue and tumour tissue. The carbon/urethane rubber mixture with different concentration of carbon is used to mimic the dielectric properties of skin, glandular structures and of the tumour. Canola oil is used to mimic fat tissue. The first of the two breast phantoms, *E1* has a skin layer, fatty tissue and a 16 mm diameter tumour located at (7 mm, 13 mm, -50.5 mm) and the second breast phantom *E2* contains a skin layer, a 4 cm diameter cylindrical glandular structure and a 16 mm tumour located at (-28 mm, 12 mm, -31 mm). The measurement data is collected using the TSAR prototype system described in [9]. Measurements are acquired at 1200 frequencies between 10 MHz and 12 GHz with a 1 kHz Intermediate Frequency (IF) bandwidth. The frequency-domain data is adjusted to compensate for antenna aperture location and is calibrated prior to the application of the artifact removal algorithm and final imaging. The calibration is performed by subtracting measurements that were collected at the same antenna positions but in the absence of the breast phantom. The calibrated frequency-domain data is then weighted with a differentiated Gaussian pulse of centre frequency 4 GHz and an approximate bandwidth of 5 GHz. Finally, an inverse Chirp-Z transform is used to convert the frequency-domain data to the time-domain for processing through the artifact removal and imaging algorithms.

4 Results

The measurement data from both experimental phantoms is processed through six imaging algorithms (described in Section 2) after preprocessing and application of the artifact removal algorithm. Three image quality metrics are computed from the resultant 3D images. The Signal-to-Clutter Ratio (SCR) is defined as the ratio of tumour intensity to clutter intensity in the 3D image. The Signal-to-Mean Ratio (SMR) is defined as the ratio of the average intensity of the tumour region to the average intensity of the overall 3D image. The localisation error is measured as a distance between the known tumour location and the detected location. Figure 1 shows images of *E2* produced with various imaging algorithms. The dominant response in each im-
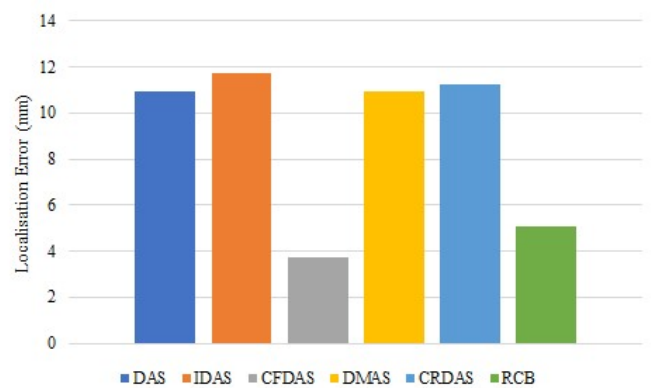

Figure 2. Localisation error averaged across both phantoms.

age is close to the actual location of the tumour. However, localisation error can be observed in each image. The images produced with all advanced algorithms have relatively lower average clutter than the conventional DAS, with the exception of CR-DAS.

Figure 2(a) shows average SMR values obtained from each imaging algorithm. On average, the IDAS provides the highest SMR value indicating best background clutter suppression capability. The SMR values of the RCB and DMAS are very similar and are only approximately 3 dB lower than the SMR value of the IDAS. While CF-DAS improves the DAS image by approximately 4 dB in terms of SMR, the CR-DAS provides same SMR value as DAS image. Figure 2(b) shows the average SCR computed for each imaging algorithm. The IDAS provided the highest SMR, however, the average SCR value of the IDAS is same as the DAS. Similarly, the CF-DAS, the CR-DAS and the RCB have lower values of SCR when compared to the DAS. The lower SCR values suggest that these algorithms also reward the secondary high intensity responses while improving the tumour response. In terms of SCR, the best performance is achieved by the DMAS.

While the IDAS achieved highest SMR, it also has the

highest localisation error as shown in Figure 2. The DMAS, CR-DAS and the DAS have same localisation error (11 mm). The CF-DAS provides lowest localisation error and the RCB has significantly lower localisation error than the DAS. It can be concluded that the IDAS, CR-DAS and the RCB significantly improve the image quality in terms of suppression of background clutter. However, DMAS is the only algorithm that significantly improves the image quality in terms of both the SMR and the SCR while keeping the localisation error same as the DAS.

5 Conclusions

In this study, the performance of a variety of DI and DA algorithms was evaluated using experimental breast phantoms. Two carbon/urethane rubber mixture based breast phantoms were scanned with the TSAR prototype at the UOFC. The measurement data was first preprocessed and the artifact was removed using the HAR algorithm. Three image quality metrics were computed from the 3D image produced with each imaging algorithm. The IDAS, CF-DAS, DMAS and RCB improved the image quality by suppressing the background clutter as compared to the DAS. However, the IDAS, CF-DAS and the RCB also improved the high intensity clutter regions resulting in the lower SCR. The DMAS algorithm was found to be the only algorithm that not only suppressed the background clutter but it also suppressed high intensity clutter regions.

Future work will investigate the performance of imaging algorithms using clinical patients.

6 Acknowledgements

References

[1] S. C. Hagness, A. Taflove, J. E. Bridges, and L. Fellow, "Two-Dimensional FDTD Analysis of a Pulsed Microwave Confocal System for Breast Cancer Detection : Fixed-Focus and Antenna-Array Sensors," *Biomedical Engineering, IEEE Transactions on*, vol. 45, no. 12, pp. 1470–1479, 1998.

[2] M. Klemm, I. J. Craddock, J. A. Leendertz, A. Preece, and R. Benjamin, "Radar-Based Breast Cancer Detection Using a Hemispherical Antenna Array Experimental Results," *Antennas and Propagation, IEEE Transactions on*, vol. 57, no. 6, pp. 1692–1704, 2009.

[3] Y. Xie, B. Guo, L. Xu, J. Li, and P. Stoica, "Multistatic adaptive microwave imaging for early breast cancer detection," *IEEE Transactions on Biomedical Engineering*, vol. 53, no. 8, pp. 1647–1657, 2006.

[4] J. Moll, C. Kexel, and V. Krozer, "A comparison of beamforming methods for microwave breast cancer detection in homogeneous and heterogeneous tissue," in *Microwave Conference (EuMC), 2013 European*, 2013, pp. 1839–1842.

[5] E. Kirshin, G. K. Zhu, M. Popovich, and M. Coates, "Evaluation of the mono-static microwave radar algorithms for breast imaging," *Proceedings of the 5th European Conference on Antennas and Propagation (EUCAP)*, pp. 881–885, 2011.

[6] D. Byrne, M. O 'Halloran, M. Glavin, and E. Jones, "Data Independent Beamforming Algorithms for Breast Cancer Detection," *Progress In Electromagnetics Research*, vol. 107, no. June, pp. 331–348, 2010.

[7] M. O'Halloran, M. Glavin, and E. Jones, "Effects of fibroglandular tissue distribution on data-independent beamforming algorithms," *Progress In Electromagnetics Research*, pp. 141–158, 2009.

[8] D. Byrne, M. O'Halloran, E. Jones, and M. Glavin, "Transmitter-grouping robust Capon beamforming for breast cancer detection," *Progress in Electromagnetics Research*, vol. 108, no. July, pp. 401–416, 2010.

[9] J. D. Garrett and E. C. Fear, "A New Breast Phantom with a Durable Skin Layer for Microwave Breast Imaging," *IEEE Transactions on Antennas and Propagation*, no. c, pp. 1–1, 2015.

[10] M. A. Elahi, A. Shahzad, M. Glavin, E. Jones, and M. O'Halloran, "Hybrid Artifact Removal for Confocal Microwave Breast Imaging," *IEEE Antennas and Wireless Propagation Letters*, vol. 13, pp. 149–152, 2014.

[11] M. A. Elahi, C. F. Curtis, E. Jones, M. Glavin, E. C. Fear, and M. O'Halloran, "Detailed Evaluation of Artifact Removal Algorithms for Radar-based Microwave Imaging of the Breast," in *2015 USNC-URSI Radio Science Meeting (Joint with AP-S Symposium)*, no. 1. IEEE, jul 2015, pp. 307–307.

[12] M. Klemm, J. A. Leendertz, D. Gibbins, I. J. Craddock, A. Preece, and R. Benjamin, "Microwave Radar-Based Breast Cancer Detection : Imaging in Inhomogeneous Breast Phantoms," vol. 8, pp. 1349–1352, 2010.

[13] M. O'Halloran, M. Glavin, and E. Jones, "Improved Confocal Microwave Imaging of the breast using path-dependent signal weighting," in *2011 30th URSI General Assembly and Scientific Symposium, URSI-GASS 2011*, 2011, pp. 1–3.